International Journal of Electrical and Computer Engineering (IJECE)
Vol. 10, No. 4, August 2020, pp. 3501~3507
ISSN: 2088-8708, DOI: 10.11591/ijece.v10i4.pp3501-3507

Enhancing the CRI and lumen output for the 6600 K WLED with convex-dual-layer remote phosphor geometry by applying red-emitting $MGSR_3SI_2O_8:EU^{2+},MN^{2+}$ phosphor

Thuc Minh Bui[1], Nguyen Thi Phuong Loan[2], Phan Xuan Le[3], Nguyen Doan Quoc Anh[4], Anh Tuan Le[5], Le Van Tho[6]
[1]Faculty of Electrical and Electronics Engineering, Nha Trang University, Vietnam
[2]Faculty of Fundamental 2, Posts and Telecommunications Institute of Technology, Vietnam
[3]Faculty of Electrical and Electronics Engineering, HCMC University of Food Industry, Vietnam
[4,5]Faculty of Electrical and Electronics Engineering, Ton Duc Thang University, Vietnam
[6]Institute of Tropical Biology, Vietnam Academy of Science and Technology, Vietnam

Article Info

Article history:

Received Oct 2, 2019
Revised Jan 18, 2020
Accepted Feb 2, 2020

Keywords:

Color rendering index
Dual-layer remote phosphor geometry
$MgSr_3Si_2O_8:Eu^{2+},Mn^{2+}$
Mie-scattering
WLEDs

ABSTRACT

The traditional white LED product established with a single chip and a single phosphor results in a low color rendering index (CRI). The upgrade of LED package is comprised of two chips and one phosphor material and gives the higher CRI while keeping high luminous efficiency. Based on previous findings, the research paper performs the application of the two chips and two phosphors to enhance the color tunability of LEDs with different amounts and intensities of the two employed phosphors. Additionally, a color design model is built to serve the purpose of bettering the color fine-tuning of the white-light LED module. The maximum value of the difference between the measured CIE 1931 color coordinates and that of the simulated model is approximately 0.0063 around the 6600 K correlated color temperature (CCT). From the results, this study offers a quick approach to achieve the color fine tuning of a white-light LED module with a high CRI and luminous efficiency.

Corresponding Author:

Anh Tuan Le
Faculty of Electrical and Electronics Engineering,
Ton Duc Thang University,
No. 19 Nguyen Huu Tho Street, Tan Phong Ward, District 7, Ho Chi Minh City, Vietnam.
Email: leanhtuan1@tdtu.edu.vn

1. INTRODUCTION

With outstanding properties of long lifespan, high reliability and endurance, eco-friendly and power-saving characteristics, and small size, white light-emitting diodes (LEDs) have a worldwide usage in illuminating applications, particularly in aspects of automatic, billboard, and low-temperature lightings [1-3]. Remarkably, their recent advances in fast switching properties have got them widely used in smart lighting which is another auto control technology. In fact, there have been a variety of methods that combine the LED chips and the phosphor to attain white light. The very first and cheapest package applying that combination consists of a single blue chip and a single yellow phosphor, but the resulted CRI is very low. Therefore, focusing on improving the CRI, the package was built with the participation of a red and a blue chip as well as a single layer of yellow phosphor. The color rendering index CRI is a quantitative measure of light quality compared to the natural light or black-body radiation. Thus, when CRI has a high value this means the applied phosphor has a broad emission spectrum which helps to better the light quality for LEDs light, similar to the continuous spectrum of the black-body radiation [4-6]. With the goal of customizing the chromaticity and CRI for LED lamps, many reports with the topics of combining phosphors with

LED chips to accomplish the optimization and prediction of the spectrum have been given. Specifically, these reports focus on the application of the empirical and mathematical models for the analysis and decomposition of the spectrum of LED chip [7-10]. Nevertheless, constructing a white LED package with tunable correlated color temperatures (CCTs), high efficiency, and superior CRI is a real challenging task to accomplish [11, 12]. Previously, the structure of a blue chip combined with two phosphor materials was applied to reach a high value of CRI, but the efficacy is poor because of the Stokes shift [13-16]. Then, the implement of the two red and blue chips together with one phosphor resulted in an increase in CRI and efficacy but was unable to tune the color, in comparison with the structure consisting of two phosphors. For those drawbacks, another white LED package comprised of the two different LED chips and two phosphors has been proposed to achieve high CRI and luminous output as well as be able to keep a tunable color. In this article, we suggest a color structure that is designed based on Beer's law and linear conversion for the demand of producing white LEDs with subtle color difference [17-21]. In addition, this W-LED module was manufactured by applying yttrium aluminum garnet (YAG) and nitride-based phosphors in blue and red LEDs with high CRI and luminous efficiency. For the WLED production, the phosphors that are mixed in silicone glues with different proportions and densities are combined with the red and blue LED chips. From the results of the article, it is possible to construct and apply this proposed color design model easily.

2. PREPARATION AND SIMULATION

2.1. Preparation

$Mg_8Ge_2O_{11}F_2:Mn^{4+}$ is a composition of the four other chemical materials, including MgO, MgF_2, $MgCO_3$, GeO_2 with the mole and weight expressed in Table 1. The preparation process of $MgSr_3Si_2O_8:Eu^{2+},Mn^{2+}$ includes two main stages of firing that need to be followed in a strict order to get the best final composition for the research. Before the first firing, four aforementioned materials must be mixed by ball-milling. Then, the attain mixture is fired in capped quartz tubes in with air at 1200^0C within two hours. Next, the fried material will be powderized by using dry ball-milling method. Finally, the powder goes through the second firing in open quartz boats overnight for about 16 hours at 1200^0C. The attain product has deep red emission color with the emission peak of 1.88 eV and the excitation efficiency of over 3.40 eV, which is beneficial enough to be applied in the simulation process.

Table 1. The ingredients of $Mg_8Ge_2O_{11}F_2:Mn^{4+}$ composition

Ingredient	Mole %	By weight (g)
MgO	700	282
MgF_2	100	62
$MgCO_3$	8	9.2
GeO_2	192	201

2.2. Simulation

The applications of the Light Tools program and Mie-theory play a crucial role in carrying out this work, as it is easier to simulate the dual-layer phosphor structure of WLED, based on the analysis of phosphor scattering phenomenon and the investigation in the impacts of $MgSr_3Si_2O_8:Eu^{2+},Mn^{2+}$ phosphor on the WLEDs' performance at the 6600 K correlated temperature. Before structuring the in-cup phosphor configuration of WLEDs, it is necessary to prepare the required phosphor layer by mixing the chemical compounding of the $MgSr_3Si_2O_8:Eu^{2+},Mn^{2+}$ phosphor and the yellow $YAG:Ce^{3+}$ with the silicon glue, as demonstrated in Figure 1. The simulated model of WLEDs includes the following constituents: nine blue chips, a reflector cup, a phosphor layer, and a silicone layer. Additionally, the parameters of each part are expressed as follows.

- A reflector with 2.07 mm depth, 8 mm bottom length and 9.85 mm top length is attached to the blue chips
- Each blue chip is designed with 1.16 W radiant power and 453 nm peak wavelength
- The refractive indexes of phosphor particles $MgSr_3Si_2O_8:Eu^{2+},Mn^{2+}$ and YAG: Ce^{3+} are set at 1.85 and 1.83 respectively

Besides, in terms of maintaining the ACCTs (average correlated color temperatures), the concentration of YAG: Ce^{3+} needs to be adjusted appropriately to the change of $MgSr_3Si_2O_8:Eu^{2+},Mn^{2+}$ concentration.

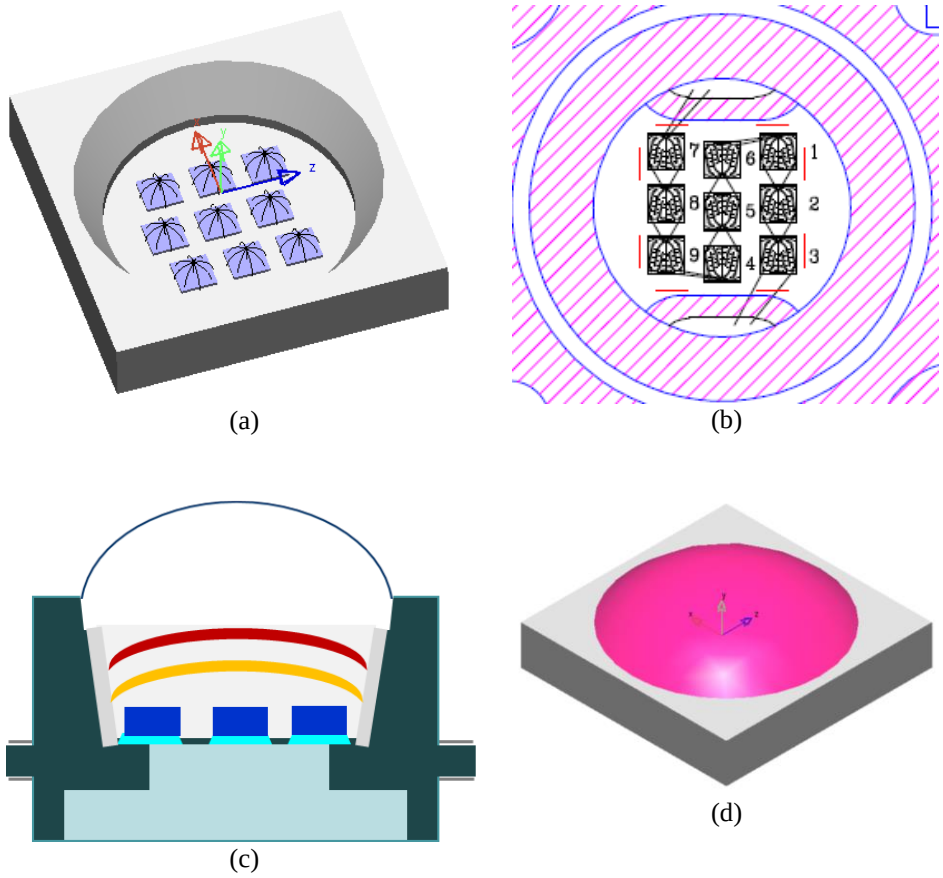

Figure 1. Illustration of WLEDs structure: (a) 3D modelling, (b) bonding diagram, (c) illustration of pc-WLEDs model, (d) simulation of WLEDs using lighttools commercial software

3. RESULTS AND DISCUSSION

As can be seen from Figure 2, the change in the concentration of red phosphor $MgSr_3Si_2O_8:Eu^{2+},Mn^{2+}$ is opposite to that of the $YAG:Ce^{3+}$ yellow phosphor. This opposite change demonstrates two aspects, the first one is to maintain the ACCTs and the second one is its influence in the scattering and absorption processes of phosphor layers inside the WLEDs, which does have a great effect on the color quality and lumen output of WLEDs. Hence, selecting the appropriate $MgSr_3Si_2O_8:Eu^{2+},Mn^{2+}$ concentration is very important as it is the factor determining the WLEDs' color quality. Vividly from the chart, when there is an increase in $MgSr_3Si_2O_8:Eu^{2+},Mn^{2+}$ concentration from 2% to 24% wt., the concentration of yellow phosphor $YAG:Ce^{3+}$ declines to retain the ACCTs, which is similar to the WLEDs structure with the ACCT of 6600 K.

Figure 3 presents the emission spectra of the WLED package with 6600 K ACCT where the impacts of different concentrations of $MgSr_3Si_2O_8:Eu^{2+}$, Mn^{2+} are demonstrated obviously. Besides, the synthesis of the spectral regions as shown in Figure 3 actually forms the white light. As can be seen, when the $MgSr_3Si_2O_8:Eu^{2+},Mn^{2+}$ concentration rises from 2% to 22%, the emission spectrum increases significantly in the wavelength range of 680 nm – 738 nm. However, this change will be insignificant if there is no spectral increase in the two range of 420 nm - 480 nm and 500 nm - 640 nm. Moreover, the growth of the spectrum in the wavelength range of 420 nm - 480 nm raises the luminous flux of blue light (blue-light scattering). Thus, it can be addressed that a higher color temperature will lead to a higher spectral emission. This result is very important to the application of $MgSr_3Si_2O_8:Eu^{2+},Mn^{2+}$ for the color quality management of the WLEDs with high color temperature. Furthermore, with these findings, the research paper could assure the ability of $MgSr_3Si_2O_8:Eu^{2+},Mn^{2+}$ in enhancing the chromatic quality of WLED packages with both low color temperature (6600 K) and high color temperature (7700 K). Therefore, the suitable $MgSr_3Si_2O_8:Eu^{2+},Mn^{2+}$ concentration is decided according to the requirements from manufacturers. If the goal is to achieve a high color quality for WLED products, a small reduction in luminous flux is acceptable.

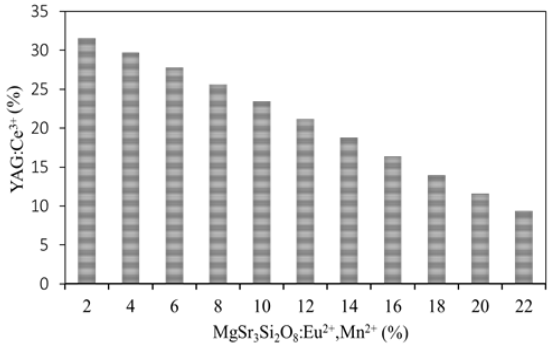

Figure 2. The change in phosphor concentration for maintaining the ACCT of WLEDs

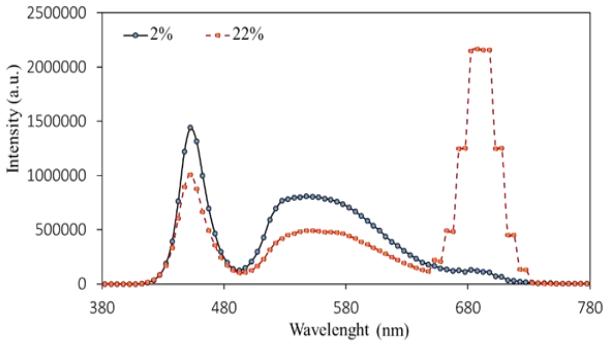

Figure 3. Emission spectra of 6600 K WLEDs with different $MgSr_3Si_2O_8:Eu^{2+},Mn^{2+}$ concentration

Demonstrated in Figure 4 is the upward trend in the color rendering index following the increase of $MgSr_3Si_2O_8:Eu^{2+}$, Mn^{2+} phosphor concentration. This trend can be explained by the absorption process of the red $MgSr_3Si_2O_8:Eu^{2+},Mn^{2+}$ phosphor layer. Specifically, as soon as the red phosphors $MgSr_3Si_2O_8:Eu^{2+},Mn^{2+}$ absorb the blue light emitted from the blue chips, they will turn these blue lights into red lights. Moreover, besides the blue light, this red phosphor $MgSr_3Si_2O_8:Eu^{2+},Mn^{2+}$ also absorbs the yellow light. However, when drawing a comparison between these two absorption processes, it has turned out that the blue light from LED chips is absorbed more strongly than the yellow light because of the absorption properties of the material, which certainly leads to the larger amount of red light components inside the WLEDs when $MgSr_3Si_2O_8:Eu^{2+},Mn^{2+}$ is added. Consequently, the color rendering index (CRI) reaches a higher value. CRI is an important factor that needs to be focused on when choosing a modern model of WLEDs, so the higher the CRI is, the more expensive the LED products become. Nonetheless, CRI cannot fully evaluate the WLEDs' color quality since it is just one of the measurement factors. Therefore, a new index called color quality scale (CQS) is introduced to be an alternative because it covers three different factors, including the CRI, the viewers' preference and the color coordinates. The CQS shows a considerable improvement with the concentration of the red phosphor $MgSr_3Si_2O_8:Eu^{2+},Mn^{2+}$, as illustrated in Figure 5. It is obvious to admit that the red phosphor $MgSr_3Si_2O_8:Eu^{2+},Mn^{2+}$ can enhance the color quality of white light LEDs with dual-layer phosphor structure. Thus, this result plays an important role in accomplishing the goal of color quality enhancement. In addition, another advantage of this type of phosphor is its low cost which is beneficial to mass production, and thus, that $MgSr_3Si_2O_8:Eu^{2+},Mn^{2+}$ is widely used in this industry can be easily understood. However, the downside when utilizing this phosphor material is that it can cause a decrease in the lumen output of WLEDs.

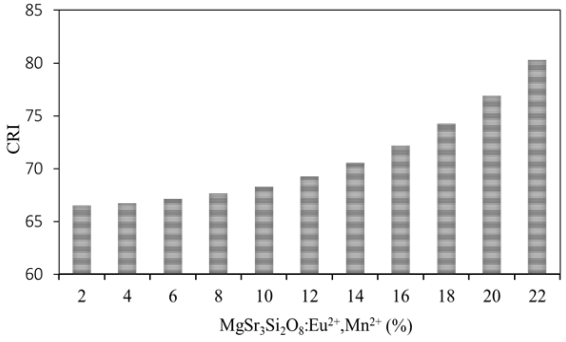

Figure 4. The color rendering index of WLEDs as a function of $MgSr_3Si_2O_8:Eu^{2+},Mn^{2+}$ concentration

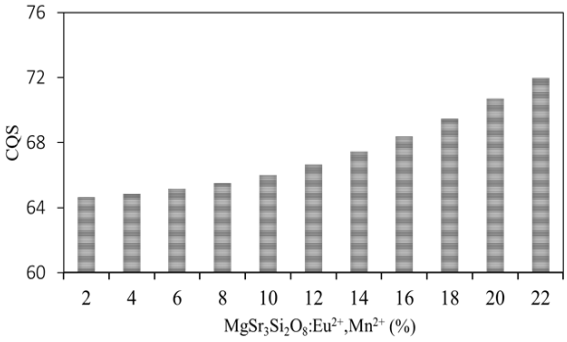

Figure 5. The color quality scale of WLEDs as a function of $MgSr_3Si_2O_8:Eu^{2+},Mn^{2+}$ concentration

In this part, we will show and explain the mathematical model of the transmitted blue light and converted yellow light in the double-layer phosphor structure to obtain a significant enhancement of the LED efficacy. The asymmetrical SPD of monochrome LED is typically modeled with Gaussian function [22, 23]:

$$P_{\lambda} = P_{opt} \frac{1}{\sigma\sqrt{2\pi}} \exp\left[-0.5 * \frac{(\lambda - \lambda_{peak})^2}{\sigma^2}\right] \quad (1)$$

where σ depends on peak wavelength λ_{peak} and FWHM $\Delta\lambda$ can be expressed as;

$$\sigma = \frac{\lambda^2{}_{peak}\Delta E}{2hc\sqrt{2\ln 2}} = \frac{\lambda^2{}_{peak}\left(\frac{hc}{\lambda_1} - \frac{hc}{\lambda_2}\right)}{2hc\sqrt{2\ln 2}} = \frac{\lambda^2{}_{peak}\left(\frac{hc\Delta\lambda}{\lambda_1\lambda_2}\right)}{2hc\sqrt{2\ln 2}} \quad (2)$$

The SPD of a white LED utilizing yellow YAG phosphor and blue LED chip can hypothetically be viewed as the aggregate of the blue and yellow spectra. However, in fact, the supposed yellow phosphor radiates light in both of the yellow and green spectra as demonstrated from the deliberate spectra in Figure 3. In the event that a blue and a yellow range are picked, the contrast between the essentially estimated SPD and twofold shading (blue and yellow shading) range model can be spoken for a green range. In this way, considering the practical circumstance, a green range can be added to the twofold range model to form the accompanying investigative tri-spectrum (B–G–Y) model represented by (3) and subsequently altered as (4).

$$\begin{aligned} P_{\lambda} &= P_{opt\_b} \frac{1}{\sigma_b\sqrt{2\pi}} \exp\left[-0.5 * \frac{(\lambda - \lambda_{peak\_b})^2}{\sigma_b{}^2}\right] \\ &+ P_{opt\_g} \frac{1}{\sigma_g\sqrt{2\pi}} \exp\left[-0.5 * \frac{(\lambda - \lambda_{peak\_g})^2}{\sigma_g{}^2}\right] \\ &+ P_{opt\_y} \frac{1}{\sigma_y\sqrt{2\pi}} \exp\left[-0.5 * \frac{(\lambda - \lambda_{peak\_y})^2}{\sigma_y{}^2}\right] \end{aligned} \quad (3)$$

$$\begin{aligned} P_{\lambda} &= \eta_b P_{opt\_total} \frac{1}{\sigma_b\sqrt{2\pi}} \exp\left[-0.5 * \frac{(\lambda - \lambda_{peak\_b})^2}{\sigma_b{}^2}\right] \\ &+ \eta_g P_{opt\_total} \frac{1}{\sigma_g\sqrt{2\pi}} \exp\left[-0.5 * \frac{(\lambda - \lambda_{peak\_g})^2}{\sigma_g{}^2}\right] \\ &+ \eta_y P_{opt\_total} \frac{1}{\sigma_y\sqrt{2\pi}} \exp\left[-0.5 * \frac{(\lambda - \lambda_{peak\_y})^2}{\sigma_y{}^2}\right] \end{aligned} \quad (4)$$

in which:
- P_{λ} Spectral power distribution (SPD) (mW/nm).
- h Planck's constant (J.s).
- c Speed of light ($m \cdot s^{-1}$).
- λ Wavelength (nm).
- P_{opt} Optical power (W).
- λ_{peak} Peak wavelength (nm).
- $\Delta\lambda$ Full-width at half-maximum (FWHM) (nm).
- η Ratio of specific spectra to white spectrum, dimensionless.
- P_{opt_b}, P_{opt_g}, P_{opt_y}, and P_{opt_total} Optical power (W) for the blue, green, yellow, and white spectra, respectively.
- λ_{peak_b}, λ_{peak_g}, and λ_{peak_y} Peak wavelengths (nm) for the blue, green, and yellow spectra, respectively.
- σ_b, σ_g, and σ_y FWHM-related coefficients (nm) for the blue, green, and yellow spectra, respectively.
- η_b, η_g, and η_y Ratios of blue–green–yellow (B–G–Y) spectra to white spectrum, respectively, dimensionless.
- λ_1, λ_2 Wavelengths at half of the peak intensity.

Therefore, the SPD modeling for the phosphor-coated white LED can be expressed as a tricolor spectrum, which can be considered as an extended Gaussian model. The scattering of $MgSr_3Si_2O_8:Eu^{2+},Mn^{2+}$ phosphor particle was analyzed by using the Mie-theory. In addition, the scattering cross section C_{sca} for spherical particles can be computed by the following expression by applying the Mie theory [24]. The transmitted light power can be calculated by the Lambert-Beer law [25]:

$$\boldsymbol{I = I_0 \exp(-\mu_{ext} L)} \quad (5)$$

where I_0, L, and μ_{ext} represent the incident light power the thickness of phosphor layer (mm), and the extinction coefficient, respectively. Moreover, the extinction coefficient can be demonstrated as the following formula: $\mu_{ext} = N_r.C_{ext}$, in which N_r indicates the number density distribution of particles (mm^{-3}), while C_{ext} (mm^2) is known as the extinction cross-section of phosphor particles.

It can be implied from (5) that the dual-layer remote phosphor results in the larger luminous efficiency for the LED packages than the single-layer phosphor. Hence, the benefit of using dual-layer remote phosphor layer in yielding better lumen output is successfully demonstrated in this study. On the other hand, the concentration of red phosphor $MgSr_3Si_2O_8:Eu^{2+},Mn^{2+}$ greatly affects the optical path of this dual-layer remote phosphor structure. Vividly, the reduction factor μ_{ext} has a direct proportion to the $MgSr_3Si_2O_8:Eu^{2+},Mn^{2+}$ concentration, but an inverse ratio to the light transmission power. Thus, as the thickness of the two phosphor layers are fixed, a decrease in luminous flux can occur with the growth of $MgSr_3Si_2O_8:Eu^{2+},Mn^{2+}$ concentration, leading to the decline in all five CCTs, as shown in Figure 6. Obviously, when the concentration of $MgSr_3Si_2O_8:Eu^{2+},Mn^{2+}$ reaches 24% wt, the luminous flux decreases dramatically. However, this drawback in lumen output can be accepted due to the great benefits that the red phosphor $MgSr_3Si_2O_8:Eu^{2+},Mn^{2+}$ brings to the WLEDs, including the better CRI and CQS. In addition, dual-layer remote phosphor can yield higher luminous flux than the single-layer phosphor without the presence of red phosphors. Therefore, the only issue here is the purpose of manufactures for determining the most appropriate phosphor concentrations of $MgSr_3Si_2O_8:Eu^{2+},Mn^{2+}$ when mass producing WLEDs products.

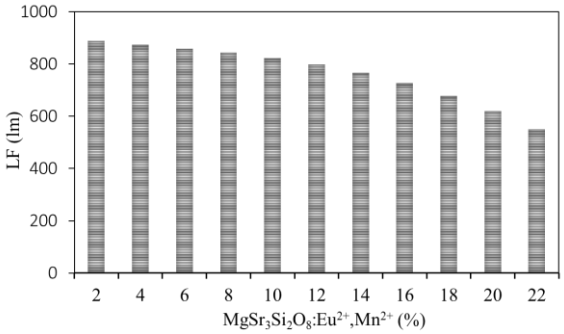

Figure 6. The luminous flux of WLEDs as a function of $MgSr_3Si_2O_8:Eu^{2+},Mn^{2+}$ concentration

4. CONCLUSION

From this article, a simple method for better performance of adjusting the color with white-light LED modules while retaining the high CRI and luminous efficacy is proposed. Depending on the manufacturers' requirements, a color design model is built based on the applications of Beer's law and linear conversion which can support the different white-light LEDs. The simulated and experimental spectra show positive overlapped results. Moreover, the biggest difference between the measured and simulated CIE 1931 color coordinates is identified by approximately 0.0063 with the 6600 K CCT. Hence, it is possible to structure the proposed color design model and get it applied easily.

REFERENCES

[1] A. A. Alatawi, *et al.*, "High-power blue superluminescent diode for high CRI lighting and high-speed visible light communication," *Optics Express*, vol. 26, no. 20, pp. 26355-26364, 2018.

[2] J. F. Ruan, *et al.*, "Phase transformation induced reversible modulation of upconversion luminescence of WO3:Yb3+, Er3+ phosphor for switching devices," *Optics Letters*, vol. 43, no. 16, pp. 3885-3888, 2018.

[3] Y. Yuan, *et al.*, "High luminous fluorescence generation using Ce:YAG transparent ceramic excited by blue laser diode," *Optical Materials Express*, vol. 8, no. 9, pp. 2760-2767, Sep. 2018.
[4] S. R. Chung, *et al.*, "Full color display fabricated by CdSe bi-color quantum dots-based white light-emitting diodes," *Optical Materials Express*, vol. 8, no. 9, pp. 2677-2686, 2018.
[5] F. Steudel, *et al.*, "Pixelated phosphors for high-resolution and high-contrast white light sources," *Optics Express*, vol. 26, no. 20, pp. 26134-26144, 2018.
[6] L. Tang, *et al.*, "Photo-induced luminescence degradation in Ce, Yb co-doped yttrium aluminum garnet phosphors," *Applied Optics*, vol. 57, no. 26, pp. 7627-7633, 2018.
[7] R. Lei, *et al.*, "Influence of excitation power and doping concentration on the upconversion emission and optical temperature sensing behavior of Er3+: BaGd2(MoO4)4 phosphors," *Optical Materials Express*, vol. 8, no. 10, pp. 3023-3035, Oct. 2018.
[8] X. Huang, *et al.*, "High-efficiency and thermally stable far-red-emitting NaLaMgWO6:Mn4+ phosphorsfor indoor plant growth light-emitting diodes," *Optics Letters*, vol. 43, no. 14, pp. 3305-3308, 2018.
[9] V. V. Bakhmet'ev, *et al.*, "Effect of copper introduction and shock-wave processing of zinc sulfide on the spectral characteristics of a manganese-activated phosphor synthesized from it," *in Journal of Optical Technology c/c of Opticheskii Zhurnal*, vol. 85, no. 6, pp. 367-370, Jun. 2018.
[10] Y. Ma, *et al.*, "Phosphor modeling based on fluorescent radiative transfer equation," *Optics Express*, vol. 26, no. 13, pp. 16442-16455, 2018.
[11] Z. Wen, *et al.*, "Fabrication and optical properties of Pr3+-doped Ba (Sn, Zr, Mg, Ta) O3 transparent ceramic phosphor," *Optics Letters*, vol. 43, no. 11, pp. 2438-2441, 2018.
[12] X. L. Song, *et al.*, "Biaxial hyperbolic metamaterials using anisotropic few-layer black phosphorus," *Optics Express*, vol. 26, no. 5, pp. 5469-5477, 2018.
[13] J. Cao, *et al.*, "Upconversion luminescence of Ba3La(PO4)3:Yb3+-Er3+/Tm3+ phosphors for optimal temperature sensing," *Applied Optics*, vol. 57, pp. 1345-1350, 2018.
[14] Y. Peng, *et al.*, "Flexible fabrication of a patterned red phosphor layer on a YAG:Ce3+ phosphor-in-glass for high-power WLEDs," *Optical Materials Express*, vol. 8, no. 3, pp. 605-614, 2018.
[15] H. Lee, *et al.*, "Phosphor-in-glass with Nd-doped glass for a white LED with a wide color gamut," *Optics Letters*, vol. 43, no. 4, pp. 627-630, 2018.
[16] T. X. Lee, *et al.*, "Miniaturized LED primary optics design used for short-distance color mixing," *Applied Optics*, vol. 55, no. 32, pp. 9067-9073, 2016.
[17] J. Gadegaard, *et al.*, "High-output LED-based light engine for profile lighting fixtures with high color uniformity using freeform reflectors," *Applied Optics*, vol. 55, no. 6, pp. 1356-1365, 2016.
[18] B. J. Chen, *et al.*, "Freeform microstructure linear light emitter design for a natural light illumination system," *Applied Optics*, vol. 54, no. 28, pp. E159-E164, 2015.
[19] S. P. Ying, *et al.*, "Improving the color uniformity of multiple colored light-emitting diodes using a periodic microstructure surface," *Applied Optics*, vol. 54, no. 28, pp. E75-E79, 2015.
[20] S. Wang, *et al.*, "Improvement in angular color uniformity of white light-emitting diodes using screen-printed multilayer phosphor-in-glass," *Applied Optics*, vol. 53, no. 36, pp. 8492-8498, 2014.
[21] W. S. Sun, *et al.*, "Compact LED projector design with high uniformity and efficiency," *Applied Optics*, vol. 53, no. 39, pp. H227-H232, Oct. 2014.
[22] M. L. Piao, *et al.*, "Achieving high levels of color uniformity and optical efficiency for a wedge-shaped waveguide head-mounted display using a photopolymer," *Applied Optics*, vol. 53, no. 10, pp. 2180-2186, 2014.
[23] K. C. Huang, *et al.*, "Improved CCT uniformity of white LED using remote phosphor with patterned sapphire substrate," *Applied Optics*, vol. 52, no. 30, pp. 7376-7381, 2013.
[24] S. Bindai, *et al.*, "Realization of phosphor-in-glass thin film on soda-lime silicate glass with low sintering temperature for high color rendering white LEDs," *Applied Optics*, vol. 58, no. 9, pp. 2372-2381, 2019.
[25] C. Huang, *et al.*, "Bandwidth correction of spectral measurement based on Levenberg–Marquardt algorithm with improved Tikhonov regularization," *Applied Optics*, vol. 58, no. 9, pp. 2166-2173, 2019.